Original Article

Magnetization and microhardness of iron−chromium alloy films electrodeposited from an aqueous solution containing N, N-dimethylformamide

Ryusei Saeki [a],[**], Taisei Yakita [b], Takeshi Ohgai [a],[b],[*]

[a] Graduate School of Engineering, Nagasaki University, Bunkyo-machi 1-14, Nagasaki, 852-8521, Japan
[b] Faculty of Engineering, Nagasaki University, Bunkyo-machi 1-14, Nagasaki, 852-8521, Japan

ARTICLE INFO

ABSTRACT

Iron-chromium (Fe−Cr) alloy films were electrochemically synthesized from an aqueous solution containing N,N-dimethylformamide (DMF). The chromium content of the alloy films increased up to ca. 32 at%, with an increase in the cathodic overpotential during the electrodeposition. Based on the XRD profiles and electron diffraction patterns, it was revealed that the electrodeposited Fe−Cr alloy films have an amorphous nanocrystalline structure. The crystal grain size of the alloys decreased due to an alloying effect of Cr atoms as well as an increase in the nucleation site density of the alloys that were electrodeposited, accompanying a significant overpotential from the stable complex ions. The saturation magnetization of the electrodeposited Fe−Cr alloy films decreased with an increase in the chromium content. On the contrary, the microhardness increased due to the synergistic contribution of solid solution strengthening and crystal grain refinement. The microhardness of the electrodeposited Fe−Cr alloy films reached up to 422.0 kgf/mm^2 (HV$_{0.05}$) and greatly exceeded that of the solidified Fe−Cr alloy ingots.

1. Introduction

Stainless steels are defined as iron-based alloys containing at least 10.5 wt% chromium [1]. These alloys can be classified into the following five categories: ferritic, austenitic, martensitic, duplex, and precipitation-hardening stainless steels—based on their chemical composition and crystalline structure. In particular, ferritic stainless steels not containing nickel atoms are known to be a promising alloy with excellent cost performance, corrosion resistance, ductility, and crashworthiness [2]. Hence, they can be used in various industrial products, such as machine structures, automobile components, and kitchen equipment [3]. Generally, Fe−Cr alloys such as ferritic stainless steels have been produced through a solidification process, but they can be also synthesized through an electrodeposition

---

process. Using electrodeposition to synthesize alloys has attracted much attention because it enables us to make an alloy film on a metallic substrate at room temperature. So far, an electrolytic bath containing hexavalent chromium (Cr^{6+}) ions has been used for electrodeposition of metallic chromium. However, it is well known that Cr^{6+} ions induce harmful environmental pollution [4,5]. In the European Union, WEEE/RoHS (Waste Electrical and Electronic Equipment/Restriction of the Use of Certain Hazardous Substances in Electrical and Electronic Equipment) directives restrict the use of Cr^{6+} ions [6]. Hence, as an alternative process, many researchers have proposed the electrodeposition of metallic chromium alloys from an electrolytic bath containing trivalent chromium (Cr^{3+}) ions (e.g., Co—Cr and Ni—Cr alloys [7], Fe—Cr alloy [8], and Fe—Cr—Ni alloy [9]). However, it is well known that the current efficiency of electrodeposition is significantly limited because the standard electrode potential of Cr/Cr^{3+} is -0.937 V (vs. Ag/AgCl/sat. KCl), which is quite less noble than that of iron-group metals (e.g., Ni/Ni^{2+}, Co/Co^{2+}, and Fe/Fe^{2+}) [10]. During the electrodeposition of less noble metals from an aqueous solution, the pH in the vicinity of the cathode increases with an increase in the current density [11]. This pH rising is caused by the high consumption rate of H^{+} ions in the vicinity of cathode due to the high rate of hydrogen gas evolution at a high current density. Hence, in a simple aqueous solution, Cr^{3+} ions will form the complexes with six water molecules ($[Cr(H_2O)_6]^{3+}$) in the vicinity of cathode at a high current density. In particular, these $[Cr(H_2O)_6]^{3+}$ ions will form a hydroxo-bridged colloidal polymer through an olation reaction in an acidic pH region (pH > 4.5) [12,13]. This colloidal polymer in the vicinity of the cathode will inhibit the electrodeposition of metallic chromium. Thus, a complex agent such as glycine, urea, or N,N-dimethylformamide (DMF) is usually added to an aqueous solution to inhibit the formation of $[Cr(H_2O)_6]^{3+}$ ions. Among these agents, DMF is well-known as an effective complex agent to reduce hydrogen evolution during the electrodeposition of metals [14]. There are several previous works concerning the structure (e.g., surface morphology and constituent phases) and corrosion resistance performance of chromium alloys which were electrodeposited from an electrolytic bath containing DMF [15–17]. However, there are few reports on the magnetic and mechanical properties of electrodeposited Fe—Cr alloy films. It is well known that the mechanical properties of metallic materials depend on their structure, such as the alloy composition and average crystal grain size. In particular, the alloy composition of electrodeposited films can be controlled by adjusting the electrolysis condition. In the case of Fe—Cr binary alloys with a Cr content of above 40%, a σ phase with brittleness will be formed easily at a high temperature [18,19]. As shown in Fig. 1, based on the binary phase diagram for the Fe—Cr system [20,21], in the temperature region from 500 to 800 °C, a σ single phase will be formed in Fe—Cr alloys with a Cr content of between 40% and 50%. Hence, it is desirable that the Cr content in Fe—Cr alloys can be controlled to less than 40%.

In the present study, Fe—Cr alloy films with a Cr content of up to 32 at% were synthesized using a potentiostatic electrodeposition technique from an aqueous solution containing DMF. The chemical state of Fe and Cr in the electrodeposited alloys was investigated, as well as the magnetization and microhardness performance.

2.   Method

Fe—Cr alloy films were fabricated using a potentiostatic electrodeposition technique from an aqueous solution (25 °C, pH 2.5) containing 0.3 M iron chloride tetrahydrate ($FeCl_2·4H_2O$), 0.5 M chromium chloride hexahydrate ($CrCl_3·6H_2O$), 0.4 M sodium chloride (NaCl), 0.4 M ammonium chloride (NH_4Cl), 0.15 M boric acid (H_3BO_3), and 5.5 M N,N-dimethylformamide (DMF) [22]. For the comparison, pure Fe films and pure Cr films were also electrodeposited from the above mixed aqueous solutions without $CrCl_3·6H_2O$ or $FeCl_2·4H_2O$, respectively. Here, the
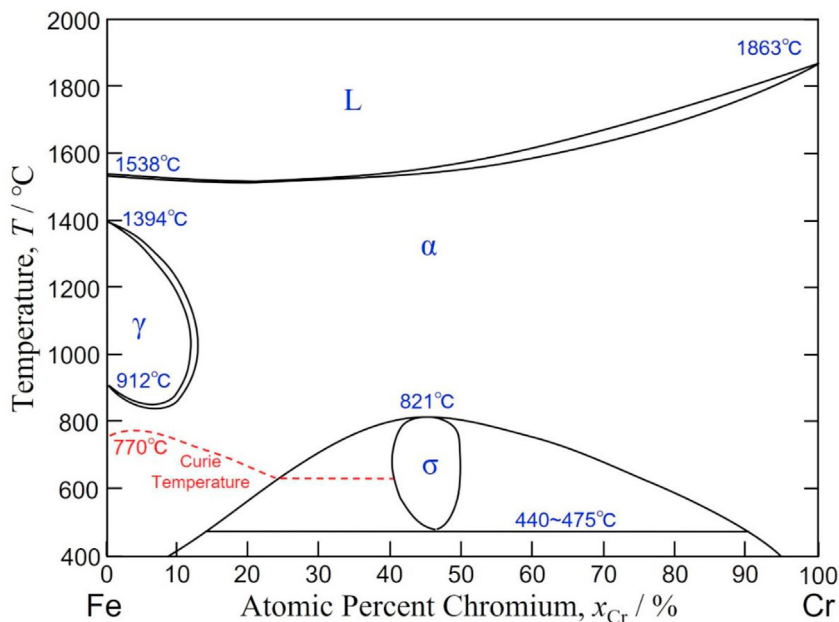

Fig. 1 — Fe—Cr binary alloys phase diagram [20,21].

aqueous solutions without $CrCl_3 \cdot 6H_2O$ or $FeCl_2 \cdot 4H_2O$ were defined as solution A and solution B, respectively, while the above mixed aqueous solution was defined as solution C. A copper foil (diameter: 6 mm) was used as a cathode for the electrodeposition of Fe−Cr alloy films. Also, a carbon rod (diameter: 3 mm, length: ca. 50 mm) and a Ag/AgCl/sat. KCl

electrode were selected as an anode and a reference electrode, respectively. Cathodic polarization curves for the solution A, B and C were obtained by using an electrochemical measurement system (HZ-7000, Hokuto Denko Corp., Tokyo, Japan). During the measurement, cathode potential was linearly scanned from −0.5 V to −2.5 V vs. Ag/AgCl/sat. KCl with the scan rate of
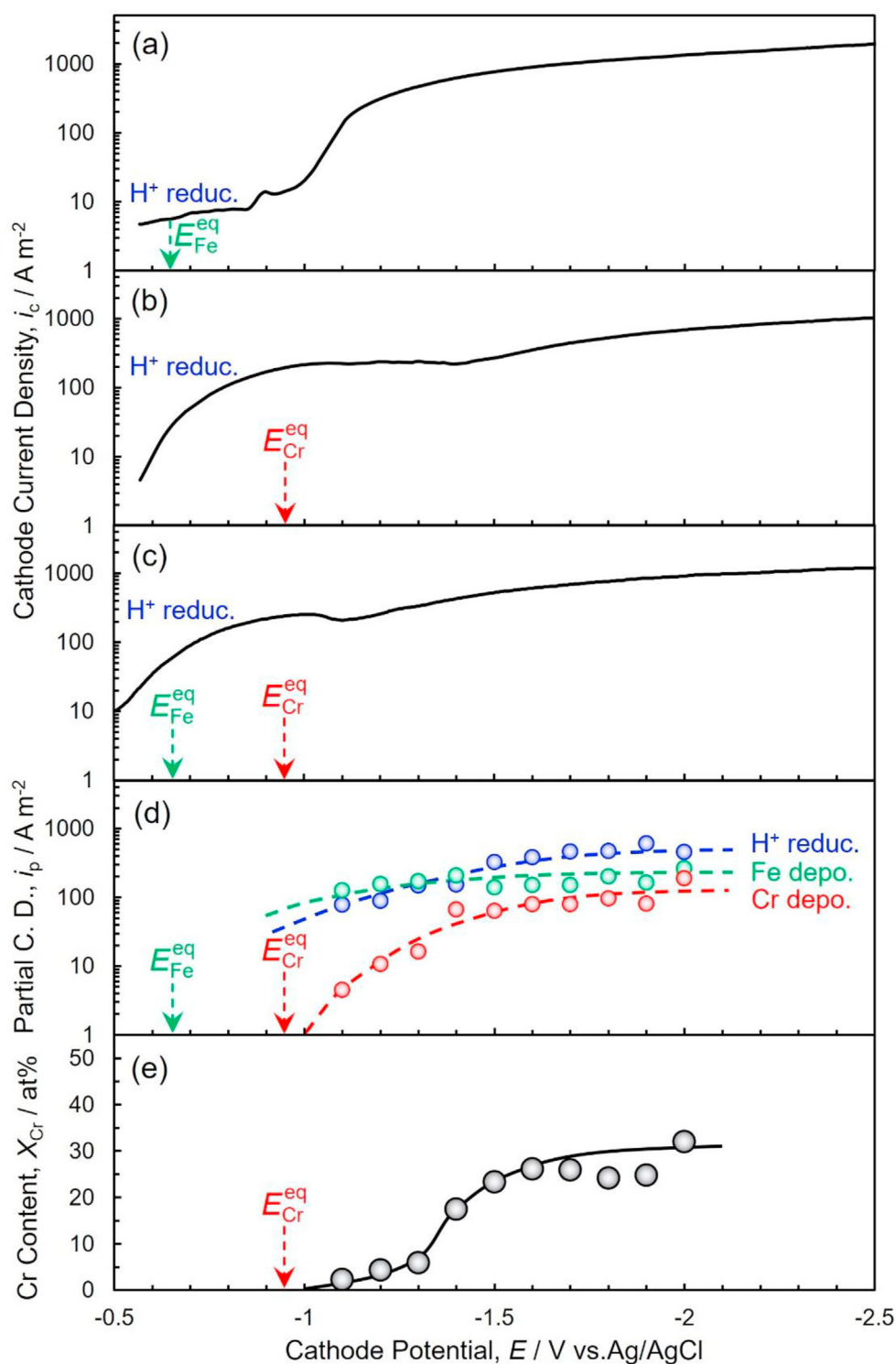
Fig. 2 − Cathodic polarization curves that were obtained from solution A (a), solution B (b), and solution C (c). Partial polarization curves (d) for Fe, Cr and H_2 reduction that were obtained from solution C (d). Effect of cathode potential on the chromium content in the electrodeposited Fe−Cr alloy films (e).

50 mV s^{-1}. Fe−Cr alloy films were prepared by using a potentiostatic electrodeposition technique with the cathode potential range from −1.1 V to −2.0 V vs. Ag/AgCl/sat. KCl. Chemical composition of the electrodeposited alloy films was determined using an energy dispersive X-ray spectrometer (EDX-800HS, Shimadzu Corp., Kyoto, Japan). Surface morphology of the electrodeposited alloy films was investigated using a field emission scanning electron microscope with an energy-dispersive X-ray spectroscopy (FE-SEM-EDS, JSM-7500FA, JEOL Ltd., Tokyo, Japan). Constituent phase and crystallinity of the electrodeposited alloy films were also investigated using an X-ray diffractometer (XRD, Miniflex 600-DX, Rigaku Corp., Tokyo, Japan) and a transmission electron microscope (TEM, JEM-2010-HT, JEOL Ltd., Tokyo, Japan). The chemical state of Fe and Cr in the electrodeposited alloy films was analyzed using an X-ray photoelectron spectroscopy (XPS, AXIS-ULTRA, Shimadzu Corp., Kyoto, Japan). Saturation magnetization of the electrodeposited alloy films was evaluated using a vibrating sample magnetometer (VSM, TM-VSM1014-CRO, Tamakawa Co., Sendai, Japan). In addition, microhardness of the electrodeposited alloy films was measured using a micro-Vickers hardness testing machine (HM-211, Mitutoyo, Kanagawa, Japan).v

3.   Results and discussion

3.1.   Electrodeposition process of Fe−Cr alloy films

Figure 2(a), (b), and (c) show the cathodic polarization curves that were obtained from solution A ([Fe^{2+}] = 0.3 M), solution B ([Cr^{3+}] = 0.5 M), and solution C ([Fe^{2+}] = 0.3 M and [Cr^{3+}] = 0.5 M), respectively. Figure 2(d) show the partial polarization curves (d) for Fe, Cr and H$_2$ reduction that were obtained from solution C using a potentiostatic electrodeposition technique for 1 h. In an aqueous solution without complexing agents, the equilibrium potentials E_{Fe}^{eq} (Fe/Fe^{2+}) and E_{Cr}^{eq} (Cr/Cr^{3+}) can be estimated as −0.652 V and −0.943 V vs.

Ag/AgCl/sat. KCl, respectively, by the following Eq. (1) (Nernst's equation) under the experimental conditions.

$$E^{eq} = E^o + \frac{RT}{nF} ln \frac{[M^{n+}]}{[M^0]} \tag{1}$$

where the standard electrode potentials, E_{Fe}^0 (−0.637 V vs. Ag/AgCl/sat. KCl) and E_{Cr}^0 (−0.937 V vs. Ag/AgCl/sat. KCl), the gas constant, R = 8.3 J K^{-1} mol^{-1}, the bath temperature, T = 298 K, the valence number of Fe^{2+} and Cr^{3+} ions, n_{Fe} = 2 and n_{Cr} = 3, Faraday constant, F = 96,485 C mol^{-1}, molar concentration of Fe^{2+} and Cr^{3+} ions, [Fe^{2+}] = 0.3 and [Cr^{3+}] = 0.5, activity of metallic Fe and Cr, [M^0] = 1. In this work, it is difficult to estimate the equilibrium potentials (M/M^{n+}) in an aqueous solution with complexing agents because there are no reliable values for stability constants on the complexes of Fe^{2+} and Cr^{3+} ions with DMF. In the previous works, it was revealed that the equilibrium potential of metals (e.g., cobalt and copper) shifted to less noble direction in an aqueous solution containing complexing agents such as citric acid and glycine due to the formation of complex species [23,24]. Hence, the equilibrium potentials E_{Fe}^{eq} (Fe/Fe^{2+}) and E_{Cr}^{eq} (Cr/Cr^{3+}) will be shifted to less noble direction when the simple and mixed complexes with DMF, NH$_3$ and Cl$^-$ are formed. In solution A (Fig. 2(a)), the slope (dlogi/dE) of the polarization curve sharply increased when the cathode potential was polarized down to around −1.0 V vs. Ag/AgCl/sat. KCl, which is quite less noble than E_{Fe}^{eq}. Bockris et al. revealed that the electrochemical reduction of iron-group metal ions (M^{2+} = Fe^{2+}, Co^{2+}, and Ni^{2+}) from an aqueous solution required a large cathodic overpotential because of the multistep reduction process via metal hydroxide ions (M(OH)$^+$) [25]. In the present study, a substantial amount of DMF was added to the electrolytic solution. Hence, the increase in the cathode current density at −1.0 V (Fig. 2(a)) seems to be caused by the reduction current of Fe^{2+} complexes with DMF. On the contrary, in solution B (Fig. 2(b)), the cathode current density increased when the cathode potential
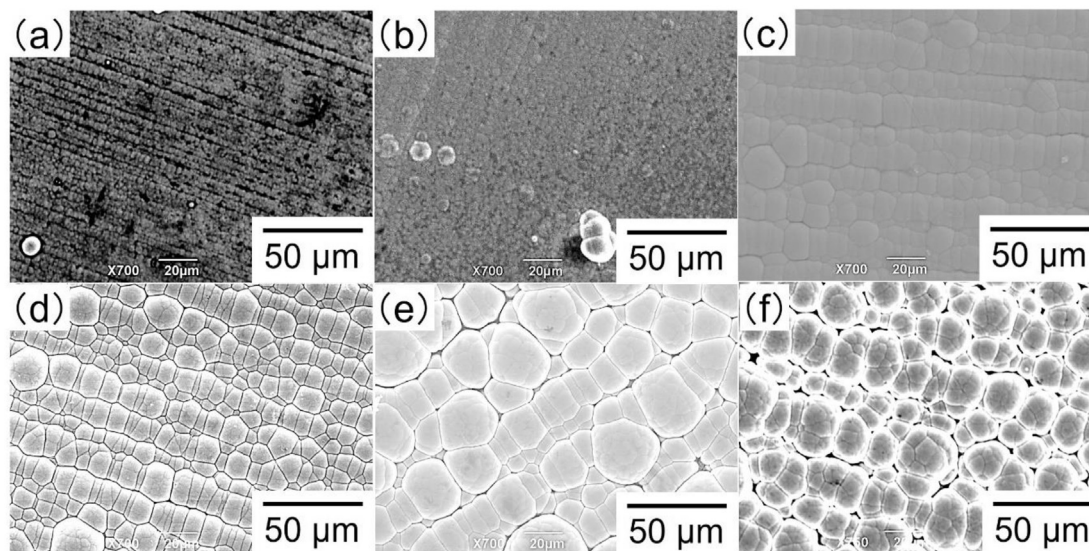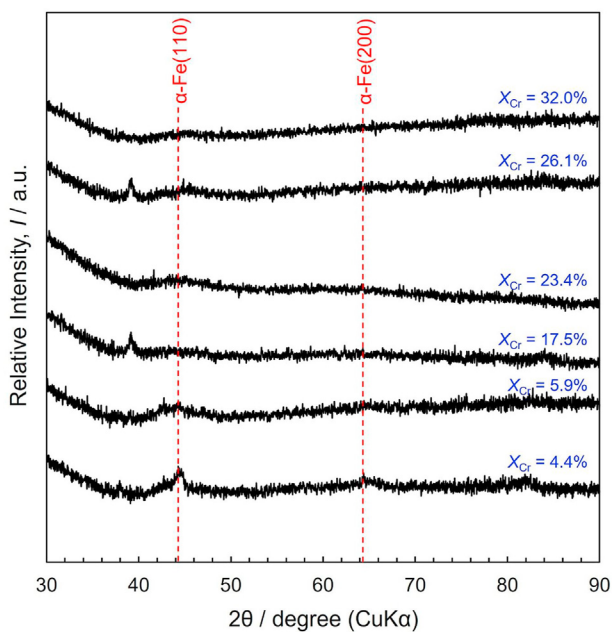

Fig. 3 − Effect of cathode potential on the SEM images of electrodeposited Fe−Cr alloy films ((a) E = −1.2 V, X$_{Cr}$ = 4.4%, (b) E = −1.3 V, X$_{Cr}$ = 5.9%, (c) E = −1.4 V, X$_{Cr}$ = 17.5%, (d) E = −1.5 V, X$_{Cr}$ = 23.4%, (e) E = −1.6 V, X$_{Cr}$ = 26.1%, (f) E = −2.0 V, X$_{Cr}$ = 32.0%).

was polarized down to around −1.4 V vs. Ag/AgCl/sat. KCl, which is quite less noble than E_{Cr}^{eq}. Zhang et al. reported that the reduction potential of Cr^{3+} ions was slightly less noble in the DMF-mixed bath compared with the aqueous bath in Cr electrodeposition [14]. They also revealed that the cathodic reduction rate clearly decreased in the DMF-mixed bath compared with the aqueous bath at below −1.0 V vs. Ag/AgCl/ sat. KCl. Hence, the increase in the cathode current density at −1.4 V (Fig. 2(b)) seems to be caused by the reduction current of Cr^{3+} complexes with DMF. Furthermore, in solution C (Fig. 2(c) and (d)), the cathode current density increased when the cathode potential was polarized down to around −1.1 V vs. Ag/AgCl/sat. KCl, which is less noble than E_{Fe}^{eq} and E_{Cr}^{eq}. Considering the cathodic polarization curve in solution A (Fig. 2(a)), the increase in the cathode current density at −1.1 V (Fig. 2(c) and (d)) seems to be caused by the reduction current of Fe^{2+} complexes with DMF.

By the way, each solution exhibited a different behavior on the reduction of H^+ ions at the cathode potential range nobler than −1.0 V. The reduction current of H^+ ions in solution A was quite smaller than that in solution B and C. Furthermore, the reduction current of H^+ ions in solution B was smaller than that in solution C. These behaviors seem to be caused by the activity of water in each solution. Considering the water of crystallization in the metal chloride chemicals ($FeCl_2 \cdot 4H_2O$ and $CrCl_3 \cdot 6H_2O$), the molar concentrations of water in solution A, B and C can be calculated to 1.2 M, 3.0 M and 4.2 M, respectively. Hence, the reduction current of H^+ ions seems to be enhanced by increasing the activity of water in solution.
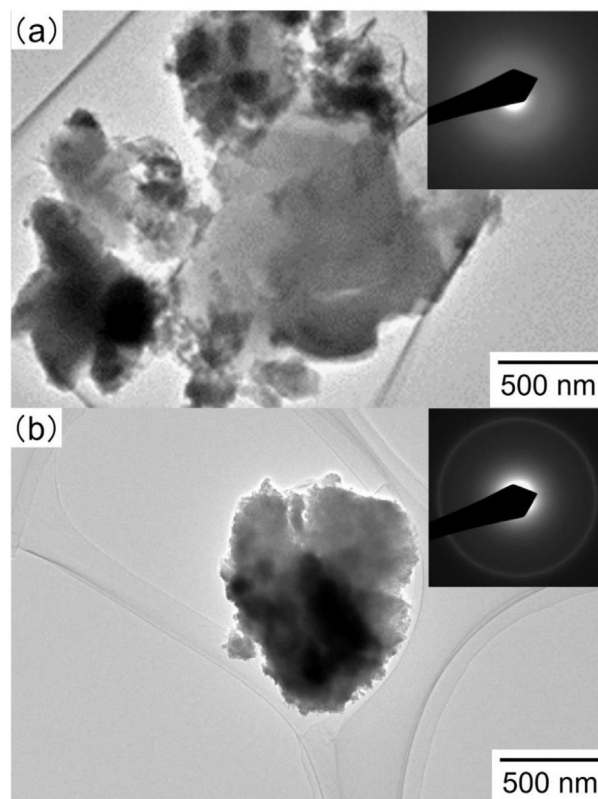
Figure 2(e) shows the effect of the cathode potential on the chromium content (X_{Cr}) in the alloy deposits that were obtained from solution C using a potentiostatic electrodeposition technique for 1 h. The chromium content in the Fe—Cr alloy films increased by shifting the cathode potential to a less noble direction. Based on the slope of polarization curve (Fig. 2(c) and (d)), the reduction rate seems to be controlled by the mass transfer step of metal ions at the cathode potentials less noble than −1.6 V vs. Ag/AgCl/sat. KCl. In this potential region, Cr content was lower than Fe content in the electrodeposited Fe—Cr alloy films, although the concentration of Cr^{3+} ions was higher than that of Fe^{2+} ions in the electrolytic bath ([Fe^{2+}] = 0.3 M, [Cr^{3+}] = 0.5 M). In a vicinity of the cathode, DMF-metal ion complexes (DMF_xFe and DMF_yCr) should be dissociated and adsorbed on the cathode. There is no reliable stability constant for DMF-metal ion complexes, however, DMF_yCr seems to be more stable than DMF_xFe under the experimental conditions. Thus, Cr^{3+} ions will emerge more slowly than Fe^{2+} ions from the complexes. Therefore, we assume that the Cr content became lower than the Fe content in the electrodeposited Fe—Cr alloy films.

In the present study, the chromium content in Fe—Cr alloy film that electrodeposited at the cathode potential of −1.1 V vs. Ag/AgCl/sat. KCl was 2.3 at%. In contrast, the chromium content reached up to 32 at% at the cathode potential of −2.0 V vs. Ag/AgCl/sat. KCl. Based on Fig. 2(d), the cathode potential region for the electrodeposition of Fe—Cr alloy films was determined to be between −1.2 V and −2.0 V vs. Ag/AgCl/sat. KCl. Thus, in the Fe—Cr system, electrochemically nobler Fe^{2+} ions preferentially deposited, rather than the less noble Cr^{3+} ions. Based on the Brenner's classification, the co-deposition behavior of Fe—Cr alloy films from a DMF bath can be categorized into the "normal co-deposition type" [26].

Fig. 4 — **Effect of chromium content on the XRD profiles of electrodeposited Fe—Cr alloy films (X_{Cr} = 4.4%, 5.9%, 17.5%, 23.4%, 26.1%, 32.0%).**

Fig. 5 — **Effect of chromium content on the TEM images and ED patterns of electrodeposited Fe—Cr alloy particles ((a) X_{Cr} = 4.4%, (b) X_{Cr} = 24.2%).**

3.2.   Structure of electrodeposited Fe–Cr alloy films

Figure 3 shows the effect of the cathode potential on the SEM images (surface morphology) of the electrodeposited Fe–Cr alloy films. As shown in Fig. 3(a), (b), and (c), the surface morphology was quite smooth in the samples that were electrodeposited at a cathode potential nobler than −1.4 V vs. Ag/AgCl/sat. KCl. In contrast, as shown in Fig. 3(d), (e), and (f), the nodule-like deposits were observed on the electro-deposited Fe–Cr alloy films that were obtained at a cathode

potential less noble than −1.4 V. As shown in Fig. 2(d), the partial current density of Fe was almost plateau at the cathode potential region less noble than −1.4 V vs. Ag/AgCl/sat. KCl. In addition, the cathode current efficiency for the alloy deposition at the cathode potential region less noble than −1.4 V was below 70%. Hence, the reduction rate of Fe^{2+} ions seems to be controlled by the mass transfer step in the potential region less noble than −1.4 V. It is well known that the dendrites or powder-like deposits are induced by a large current density with a diffusion limit. Hence, in this potential region, the
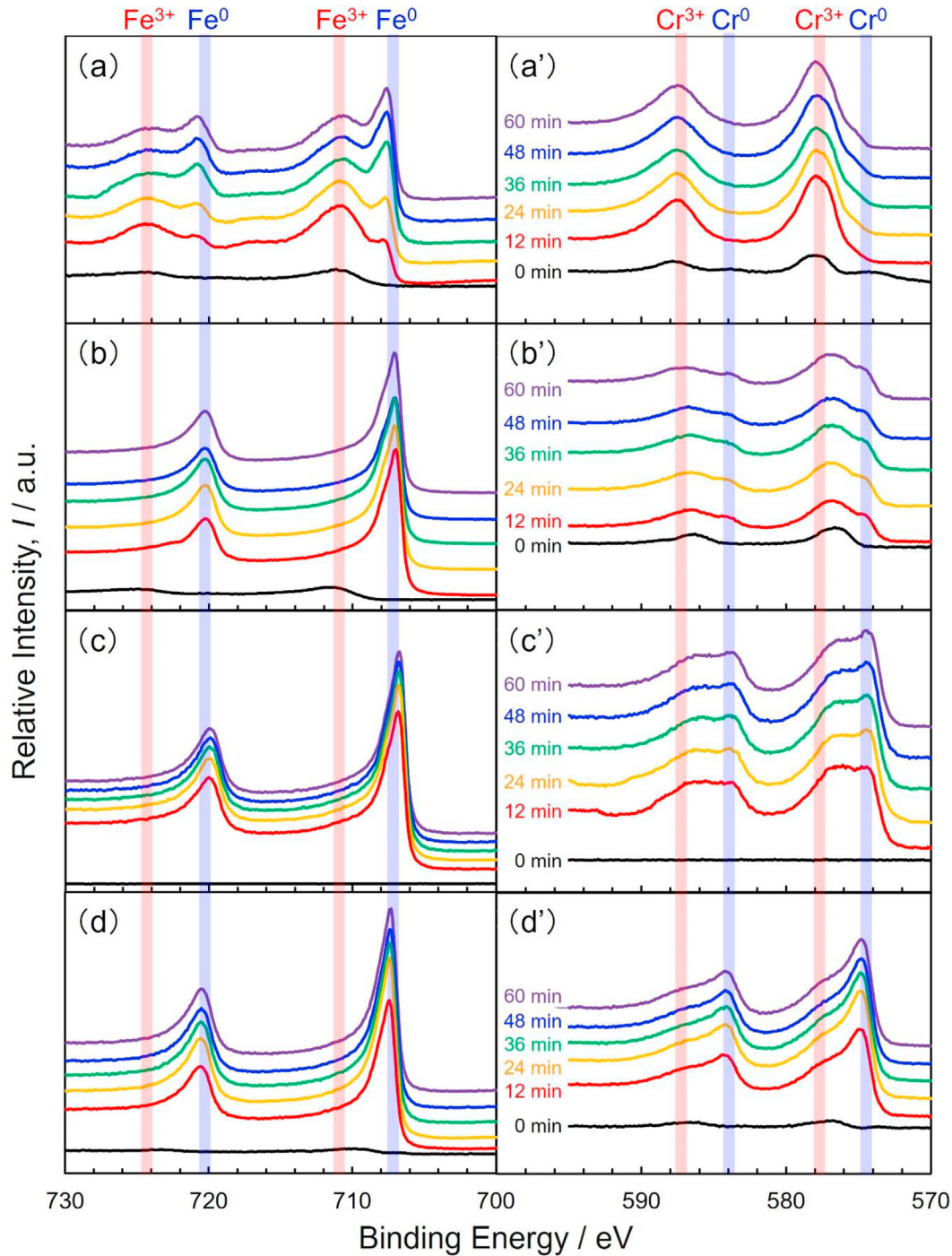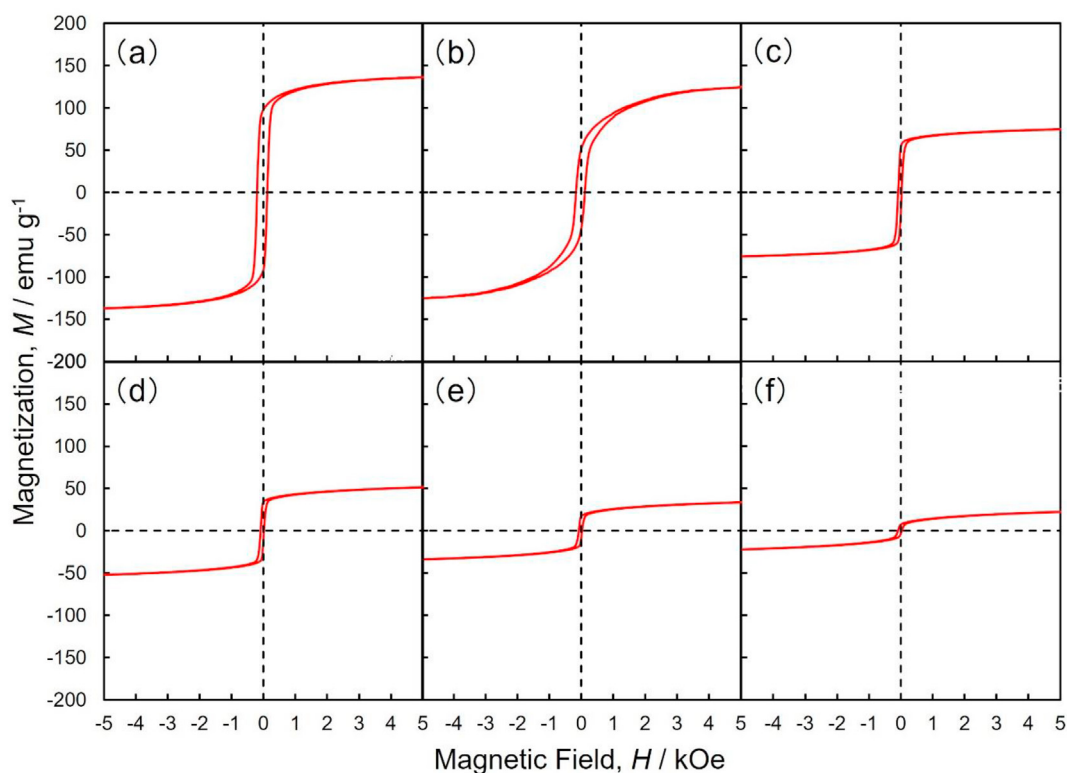

Fig. 6 – Effect of chromium content on the XPS profiles of electrodeposited Fe–Cr alloy films ((a), (a') X_{Cr} = 4.4%, (b), (b') X_{Cr} = 17.5%, (c), (c') X_{Cr} = 26.0%, (d), (d') X_{Cr} = 32.0%).

formation of nodule-like deposits seems to be caused by a non-uniform nucleation process on the cathode with a diffusion limit of Fe^{2+} ions as well as the presence of Cr in the alloy films (Fig. 3(d), (e), and (f)). Figure 4 shows the effect of chromium content on the XRD profiles of the electrodeposited Fe–Cr alloy films. The broad peaks associated with α-Fe (110) and (200) were observed at 2θ of around 44° and 64°, respectively [27]. Hence, the electrodeposited Fe–Cr alloys seem to be composed of an amorphous phase. Wang et al. reported that electrodeposited Fe–Cr alloys with a Cr content of above 22.9 at% were composed of an amorphous phase, while those with a Cr content of below 22.4 at% were composed of a metastable phase [8]. In the present study, even in the sample with a Cr content of 4.4 at%, an amorphous phase was revealed due to the formation of metal ions complexes with DMF. Figure 5 shows the TEM images and electron diffraction (ED) patterns of the electrodeposited Fe–Cr alloy films ((a) $X_{Cr} = 4.4$ at%, (b) $X_{Cr} = 24.2$ at%). According to the ED patterns, concentric and vague patterns (halo-patterns) were observed [28]. Hence, it was confirmed that the electrodeposited Fe–Cr alloy films have an amorphous phase. This amorphous phase formation in the electrodeposited Fe–Cr alloys seems to be induced through the electrochemical reduction process of metal complex ions (M^{n+}-DMF) with a large overpotential, as shown in Fig. 2(c) and (d). Figure 6 shows the effect of cathode potential on the XPS profiles of electrodeposited Fe–Cr alloy films. Based on these XPS profiles, the chemical state of iron and chromium can be estimated. Idczak et al. reported that the binding energies of metallic iron (Fe^0), iron oxide (Fe^{3+}),

metallic chromium (Cr^0), and chromium oxide (Cr^{3+}) corresponded to 707.3 eV (Fe^0-$2p_{3/2}$), 710.7 eV (Fe^{3+}-$2p_{3/2}$), 574.8 eV (Cr^0-$2p_{3/2}$), and 577.9 eV (Cr^{3+}-$2p_{3/2}$), respectively [29]. In the present study, the Fe–Cr alloy film ($X_{Cr} = 4.4$ at%) that was electrodeposited at −1.2 V (Fig. 6(a)) was a composite mixture of metallic iron (Fe^0), iron oxide (Fe^{3+}), and chromium oxide (Cr^{3+}). In contrast, the Fe–Cr alloy film ($X_{Cr} > 17.5$ at%) that was electrodeposited at a cathode potential below −1.4 V (Fig. 6(b), (c), and (d)) was composed of metallic iron (Fe^0), metallic chromium (Cr^0), and chromium oxide (Cr^{3+}). Hence, in the present study, it was necessary to control the cathode potential to below −1.4 V vs. Ag/AgCl/sat. KCl for the electrodeposition of the metallic Fe–Cr alloy-based composite films.

3.3. Magnetic and mechanical properties of electrodeposited Fe–Cr alloy films

Figure 7 shows the magnetic hysteresis loops of the electrodeposited Fe–Cr alloy films. An external magnetic field was applied to in-plane direction to the electrodeposited films. As shown in Fig. 6, the electrodeposited Fe–Cr alloy films exhibited a typical soft magnetic performance [30]. Based on the magnetic hysteresis loops, the saturation magnetization and coercivity were determined. Figure 8(a) and (b) show the effect of chromium content (X_{Cr}) on the saturation magnetization (M_s) and coercivity (H_c) of the Fe–Cr alloy films, respectively. It was revealed that M_s and H_c decreased with an increase in X_{Cr}. The direct exchange interaction between iron atoms seems to decline due to an increase in the concentration

Fig. 7 – **Effect of chromium content on the magnetic hysteresis loops of electrodeposited Fe–Cr alloy films ((a) $E = −1.2$ V, $X_{Cr} = 4.4\%$, (b) $E = −1.3$ V, $X_{Cr} = 5.9\%$, (c) $E = −1.4$ V, $X_{Cr} = 17.5\%$, (d) $E = −1.5$ V, $X_{Cr} = 23.4\%$, (e) $E = −1.6$ V, $X_{Cr} = 26.1\%$, (f) $E = −2.0$ V, $X_{Cr} = 32.0\%$). An external magnetic field was applied to in-plane direction to the electrodeposited alloy films.**
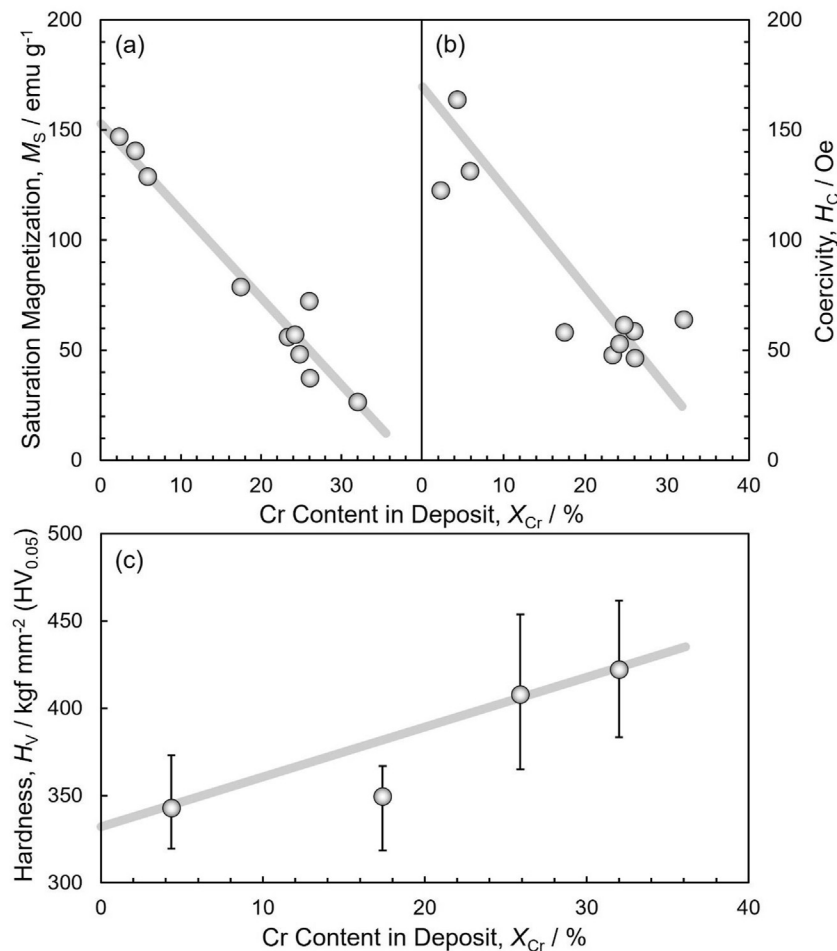
Fig. 8 — Effect of chromium content on the saturation magnetization (a), coercivity (b) and microhardness (c) of electrodeposited Fe—Cr alloy films.

of chromium atoms. In addition, an antiferromagnetic coupling is also assumed between iron and chromium atoms [31]. Bertero et al. reported that Fe—Cr—Ni alloys with chromium concentrations between 4.1 and 41.0 wt.% were able to be electrodeposited from an aqueous solution containing glycine. They revealed that the saturation magnetization of the electrodeposited Fe—Cr—Ni alloys decreased with an increase in the chromium content up to 41.0 wt% [32]. Hence, as shown in Fig. 8(a), the results in the present study are consistent with their report. It is well known that the coercivity of ferromagnetic metals decreases with decreasing the average crystal grain size in a superparamagnetic domain structure [33,34]. Therefore, the decrease in coercivity (Fig. 8(b)) seems to be caused by the decrease in the average cluster size and its short-range ordering due to an increase in the overvoltage and current density of reaction deposition alloys and an increase in the chromium content, as shown in Figs. 4 and 5. Figure 8(c) shows the effect of chromium content on the microhardness of the electrodeposited Fe—Cr alloy films. The microhardness increased with an increase in chromium content, as shown in Fig. 8(c). Mohapatra et al. and Noshita et al. reported that the microhardness of Fe—Cr alloys that were synthesized by a melting method ranged from ca. 60 to 150 kgf/mm^2 with an

increase in chromium content up to around 30wt.% [35,36]. In the present study, the microhardness of the electrodeposited Fe—Cr alloy films increased up to 422.0 kgf/mm^2 (X_{Cr} = 32.0 at %). Based on the mechanism of solid solution strengthening, a substantial lattice strain is introduced into a metallic crystal when the solvent atoms (i.e., iron atoms) are replaced by the solute atoms (i.e., chromium atoms). The amount of lattice strain increases with an increase in the concentration of the solute atoms. The strength of metallic materials increases due to the interaction between the dislocation and lattice strains. In addition, the crystal grain boundary area increases with a decrease in the average crystal grain size. According to the strengthening mechanism due to the crystal grain refinement, the movement of dislocation along the sliding plane is inhibited by the grain boundaries. In the present study, the microhardness of the electrodeposited Fe—Cr alloy films seems to be improved due to the synergistic contribution of solid solution strengthening and crystal grain refinement. The microhardness will be improved when the chromium content is further increased to above 40 at%. However, based on the binary phase diagram of the Fe—Cr system shown Fig. 1 [20,21], a hard and brittle σ single phase will be formed by the annealing process at temperatures above 500 °C.

4. Conclusion

Fe–Cr binary alloy films with a chromium content ranging from 2.3% to 32.0 at% were synthesized using a potentiostatic electrodeposition technique from an electrolytic bath containing N,N-dimethylformamide (DMF). The chromium content in the electrodeposited Fe–Cr alloy films increased by shifting the cathode potential in a less noble direction during the electrodeposition process. According to the XRD profiles and electron diffraction patterns, it was revealed that the Fe–Cr alloy films have an amorphous phase. Metallic Fe–Cr alloy-based composite films were obtained by controlling the cathode potential in a range below −1.4 V vs. Ag/AgCl/sat. KCl. The saturation magnetization and coercivity of the electrodeposited Fe–Cr alloy films decreased with an increase in the chromium content. In contrast, the microhardness reached up to 422.0 kgf/mm^2 with an increase in the chromium content up to 32.0 at%.

Authors' contributions

R.S and T.Y carried out experiments, analyzed data, and wrote manuscript. T.O. designed the study, supervised the project, and analyzed data. All authors read and approved the final manuscript.

Declaration of Competing Interest

The authors declare that they have no competing interests.

Acknowledgements

REFERENCES

[1] Moon J, Ha HY, Kim KW, Park SJ, Lee TH, Kim SD, et al. A new class of lightweight, stainless steels with ultra-high strength and large ductility. Sci Rep 2020;10:12140.

[2] Cashell KA, Baddoo NR. Ferritic stainless steels in structural applications. Thin-Walled Struct 2014;83:169–81.

[3] Wang Z, Wu T, Ru J, Hua Y, Bu J, Wang D. Eco-friendly preparation of nanocrystalline Fe-Cr alloy coating by electrodeposition in deep eutectic solvent without any additives for anti-corrosion. Surf Coating Technol 2021;406:126636.

[4] Danilov FI, Protsenko VS, Gordiienko VO, Kwon SC, Lee JY, Kim M. Nanocrystalline hard chromium electrodeposition from trivalent chromium bath containing carbamide and formic acid: structure, composition, electrochemical corrosion behavior, hardness and wear characteristics of deposits. Appl Surf Sci 2011;257:8048–53.

[5] Eugénio S, Rangel CM, Vilar R, do Rego AMB. Electrodeposition of black chromium spectrally selective coatings from a Cr(III)–ionic liquid solution. Thin Solid Films 2011;519:1845–50.

[6] Huang CA, Chang JH, Chen CY, Liao KY, Mayer J. Microstructure and electrochemical corrosion behavior of Cr–Ni–Fe alloy deposits electroplated in the presence of trivalent Cr ions. Thin Solid Films 2013;544:69–73.

[7] Ohgai T, Tanaka Y, Fujimaru T. Soft magnetic properties of Ni–Cr and Co–Cr alloy thin films electrodeposited from aqueous solutions containing trivalent chromium ions and glycine. J Appl Electrochem 2012;42:893–9.

[8] Wang F, Itoh K, Watanabe T. Relationship between the crystallographic structure of electrodeposited Fe–Cr alloy film and its thermal equilibrium diagram. Mater Trans 2002;43:439–42.

[9] Bertero E, Manzano CV, Bürki G, Philippe L. Stainless steel-like FeCrNi nanostructures via electrodeposition into AAO templates using a mixed-solvent Cr(III)-based electrolyte. Mater Des 2020;190:108559.

[10] Adachi K, Kitada A, Fukami K, Murase K. Crystalline chromium electroplating with high current efficiency using chloride hydrate melt-based trivalent chromium baths. Electrochim Acta 2020;338:135873.

[11] Nakano H, Ohgai T, Fukushima H, Akiyama T, Kammel R. Factors determining the critical current density for zinc deposition in sulfate solutions. Metall 2001;55:676–81.

[12] Giovanardi R, Orlando G. Chromium electrodeposition from Cr(III) aqueous solutions. Surf Coating Technol 2011;205:3947–55.

[13] Saravanan G, Mohan S. Corrosion behavior of Cr electrodeposited from Cr(VI) and Cr(III)-baths using direct (DCD) and pulse electrodeposition (PED) techniques. Corros Sci 2009;51:197–202.

[14] Zhang H, Liu L, Bai J, Liu X. Corrosion behavior and microstructure of electrodeposited nano-layered Ni–Cr coatings. Thin Solid Films 2015;595:36–40.

[15] El-Sharif M, Wang X, Chisholm CU, Watson A, Vertes A, Kuzmann E. Effect of heat treatment on microstructure of Cr-Ni-Fe coatings prepared by electrodeposition. Mater Sci Forum 1994;163–166:633–8.

[16] Kuznetsov VV, Filatova EA, Telezhkina AV, Kruglikov SS. Corrosion resistance of Co–Cr–W coatings obtained by electrodeposition. J Solid State Electrochem 2018;22:2267–76.

[17] Philippe L, Heiss C, Michler J. Electroplating of stainless steel. Chem Mater 2008;20:3377–84.

[18] Yamagishi T, Akita M, Nakajima M, Uematsu Y, Tokaji K. Effect of σ-phase embrittlement on fatigue behaviour in high-chromium ferritic stainless steel. Procedia Eng 2010;2:275–81.

[19] Park CJ, Ahn MK, Kwon HS. Influences of Mo substitution by W on the precipitation kinetics of secondary phases and the associated localized corrosion and embrittlement in 29% Cr ferritic stainless steels. Mater Sci Eng, A 2006;418:211–7.

[20] Al-Mangour B. Powder metallurgy of stainless steel: state-of the art, challenges, and development. In: Stainless steel: microstructure, mechanical properties and methods of application. Nova Science Publishers; 2015. p. 37–80.

[21] Okamato H. Binary alloy phase diagrams. 2nd ed. ASM International; 1990.

[22] Furukawa N, Hayashi T. Electrodeposition of iron-chromium alloys from an aqueous dimethylformamide bath. J Met Finish Soc Jpn 1978;29:301–6.

[23] Saeki R, Ohgai T. J Mater Res Technol 2020;9(4):8029–40.

[24] O'Connor GM, Lepkova K, Eksteen JJ, Oraby EA. Hydrometallurgy 2018;181:221–9.

[25] Bockris JO'M, Kita H. Analysis of galvanostatic transients and application to the iron electrode reaction. J Electrochem Soc 1961;108:676–81.

[26] Zangari G. Electrodeposition of alloys and compounds in the era of microelectronics and energy conversion technology. Coatings 2015;5(2):195–218.

[27] Neetzel C, Ohgai T, Yanai T, Nakano M, Fukunaga H. Uniaxial magnetization performance of textured Fe nanowire arrays electrodeposited by a pulsed potential deposition technique. Nanoscale Res Lett 2017;12:598.

[28] Ohgai T, Tanaka Y, Washio R. Nanocrystalline structure and soft magnetic properties of nickel–molybdenum alloy thin films electrodeposited from acidic and alkaline aqueous solutions. J Solid State Electrochem 2013;17:743–50.

[29] Idczak K, Idczak R. Investigation of surface segregation in Fe-Cr-Si alloys by XPS. Metall Mater Trans A 2020;51A:3076–89.

[30] Ohgai T, Washio R, Tanaka Y. Anisotropic magnetization behavior of electrodeposited nanocrystalline Ni-Mo alloy thin films and nanowires array. J Electrochem Soc 2012;159:H800–4.

[31] Atalay S, Gencer H, Kolat VS. Magnetic entropy change in $Fe_{74-x}Cr_xCu_1Nb_3Si_{13}B_9$ (x = 14 and 17) amorphous alloys. J Non-Cryst Solids 2005;351:2373–7.

[32] Bertero E, Hasegawa M, Staubli S, Pellicer E, Herrmann IK, Sort J, et al. Electrodeposition of amorphous Fe-Cr-Ni stainless steel alloy with high corrosion resistance, low cytotoxicity and soft magnetic properties. Surf Coating Technol 2018;349:745–51.

[33] Herzer G. Grain size dependence of coercivity and permeability in nanocrystalline ferromagnets. IEEE Trans Magn 1990;26:1397–402.

[34] Ohgai T, Fujimaru T, Tanaka Y. Isotropic magnetization response of electrodeposited nanocrystalline Ni–W alloy nanowire arrays. J Appl Electrochem 2014;44:301–7.

[35] Mohapatra JN, Kamada Y, Kikuchi H, Kobayashi S, Echigoya J, Park DG, et al. Study of thermal ageing behaviour of Fe-Cr model alloys by magnetic hysteresis loop technique. J Phys Conf Ser 2011;266:12041.

[36] Noshita Y, Sato K, Yamashita H, Kasada R, Xu Q, Hatakeyama M, et al. Detection of phase separation of neutron-irradiated Fe–Cr binary alloys using positron annihilation spectroscopy. Nucl Mater Energy 2018;15:175–9.